PERGAMON

International Journal of Heat and Mass Transfer 44 (2001) 131–142

International Journal of HEAT and MASS TRANSFER

www.elsevier.com/locate/ijhmt

Application of narrow and wide band models for radiative transfer in planar media

J.G. Marakis

Institute of Fluid Mechanics, University of Erlangen–Nürnberg, Cauerstrasse 4, D91058 Erlangen, Germany

Received 9 August 1999; received in revised form 22 February 2000

Abstract

A ray tracing formulation is described for the solution of the radiative heat transfer equation in absorbing, emitting and non-scattering real gases. The Goody and the Malkmus statistical narrow band models and the Edwards wide band model are used for calculating the radiative dissipation and the wall fluxes in a series of planar configurations containing inhomogeneous, non-isothermal H_2O/N_2 mixtures bounded by non-reflecting walls. Comparisons between these models are performed and their sensitivity on the sets of the band parameters is investigated. The accuracy of the results obtained by considering correlated and non-correlated solutions is also discussed.

Keywords: Participating media; Radiation; Thermophysical

1. Introduction

There is a great variety of engineering applications where thermal radiation is an important heat transfer mode. Among these applications are various combustion configurations, detection of infrared heat sources and high temperature heat exchangers. In order to determine the distributions of the radiative fluxes and source terms in these applications, a method is required for the solution of the Radiative Transfer Equation (RTE) and a model for the calculation of the radiative properties of the gas phase. These requirements are not independent from each other since the property included in the RTE is the absorption coefficient, while the available radiative property models provide either transmissivity or absorption coefficient. Two modelling approaches can be distinguished. The first approach is oriented towards the determination of the absorption coefficient, the property which is usually adopted in RTE solution methods. The second approach, followed in the present study, rewrites RTE in terms of transmissivity, the property that can be calculated by a band model.

Many models are included in the first approach. The Weighted-Sum-of-Gray-Gases (WSGG) model, originally developed by Hottel and Sarofim [1] for the zonal method, is a representative of this category, especially after the work of Modest [2] who demonstrated its use in media characterised by a constant absorption coefficient and black walls. Song [3] proposed a modification of the WSGG model by explicitly specifying the spectral region occupied by each gray gas. Parameters for the WSGG model have been published by Foster and Taylor [4], Smith et al. [5] and Soufiani and Djavdan [6]. The application of WSGG models in the

E-mail address: jmarakis@1stm.uni-erlangen.de (J.G. Marakis).

0017-9310/01/$ - see front matter
PII: S0017-9310(00)00090-9

Nomenclature

a	mean line-width to spacing parameter
A^*	dimensionless band absorption
d	mean spectral line spacing in $\Delta\nu$
k	mean line intensity to line spacing
L	slab thickness
N	number of intersection points
q	radiative flux
s	direction of a ray
S	mean line intensity in $\Delta\nu$
u	optical length
x	normal direction

Greek symbols

β	line overlap parameter
γ	line width
$\Delta\vartheta$	angular interval
$\Delta\nu$	frequency interval
ϑ	polar angle
κ	absorption coefficient
μ	direction cosine
τ	transmissivity

Subscripts

0	grid point at west wall
b	blackbody
E	Edwards EWB model
G	Goody SNB model
H	band head
i	frequency index
j, k	spatial indices
m	angular index
M	Malkmus SNB model
n	ray element
N	grid point at east wall
s	space variable
w	wall
x	normal direction
ν	frequency

Superscripts

$\bar{}$	spectrally averaged
$\tilde{}$	scaled quantity

Abbreviations

CG	Curtis–Godson
CK	correlated k-distribution
EWB	exponential wide band
HITRAN	high resolution transmission molecular database
HL^{2}ST	Hartmann, Levi Di Leon, Soufiani, Taine
LBL	line-by-line
LMRT	Ludwig, Malkmus, Reardon, Thompson
RMC	reverse Monte Carlo
RTE	radiative transfer equation
SLW	spectral line weighted sum of gray gases
SNB	statistical narrow band
WSGG	weighted sum of gray gases

frame of combustion simulations is comprehensively reviewed in Lallemant et al. [7]. As it is shown in Soufiani and Djavdan [6] and Pierrot et al. [8], the WSGG model, though it has the lowest computational requirements compared to other models, it also exhibits the poorest accuracy and sometimes unpredictable behaviour.

To circumvent these inefficiencies, Goody et al. [9] and Lacis and Oinas [10] introduced the correlated k-distribution (CK) method which effectively combines the estimation of the absorption coefficient with the band subdivision of the spectrum. Model parameters and curve fits for the CK-method are given in Soufiani et al. [11] for spectral intervals in the order of a few tenths cm^{-1} and in Marin and Buckius [12–14] for spectral intervals in the order of an entire ro-vibrational band. A model that can be classified in between the WSGG and the CK-methods is the Spectral Line Weighted Sum of Gray Gases (SLW) model of Denison and Webb [15–17]. This model calculates the weights in a sum of gray gases using the blackbody absorption line distribution function, which represents the fraction of the blackbody radiation emitted in the spectral regions where the absorption coefficient is less than a prescribed value.

Another method that directly determines the absorption coefficient is the Line-By-Line (LBL) calculation (Taine [18], Hartmann et al. [19], Riviere et al. [20]). In this method, the absorption coefficient is estimated at spectral locations by summing up the contributions of all the neighbouring spectral lines within a given range. The intervals between the evaluation locations should be an order of magnitude finer than the line widths. A database containing the necessary data for LBL calculations is the High Resolution Transmission Molecular Database (HITRAN) (Rothman et al. [21]). High temperature H_2O/CO_2 spectra can be handled using the

HITEMP extension [22]. At the resolution of the LBL calculations, the spectral absorption coefficient and the spectral transmissivity are related through Beer's law and therefore, LBL effectively belongs to both modelling approaches.

The second approach, which is adopted in this work, is based on the integral form of the RTE. In this approach, RTE is rewritten in terms of a mean over a spectral range transmissivity, the property that can be calculated by the narrow and wide band models. A difference between these two kinds of models is the spectral resolution. In addition, narrow band models attempt to estimate transmissivity at distinct spectral intervals by taking into account the contributions of all the significant spectral lines, irrespective of the band system they belong to. In contrast, wide band models attempt to estimate a radiative property that characterises all the rotational lines corresponding to a given vibrational transition.

In the present study, two Statistical Narrow Band (SNB) models are examined. This category of models is based on the hypothesis made by Goody [23] that the positioning of independent lines within subdivisions of the infrared spectrum is random. It is noteworthy that the validity of this hypothesis increases at high temperatures where the growth of spectral lines belonging to non-ground transitions extends the potential for band overlapping. To construct an SNB model, two additional assumptions are needed. The first one concerns the profile of the spectral lines and the second one, a distribution function for the line intensities. In all the applications where collision broadening is dominant, the Lorentz profile is accepted. For the second assumption, Goody [23] adopted an exponential-tailed line intensity distribution and Malkmus [24] an exponential-tailed inverse one. Subsequently, the two SNB models that are derived from the two intensity distributions of Lorentz lines will be named Goody and Malkmus models. The Goody model is the basis of the RADCAL code (Grosshandler [25]). Applications of this code are reported by Grosshandler and Nguyen [26], Kounalakis et al. [27] and Fuss et al. [28]. It has also been used for the estimation of the WSGG parameters in Ref. [4] and by Leckner [29] for polynomial fits of the H_2O/CO_2 total emissivity. The Malkmus model was the subject of a series of studies by Soufiani, Taine and co-workers. These include the estimation of narrow band parameters (Refs. [19,30], newer set in [11,20]), WSGG parameters (Ref. [6]), combined radiation and convection [31,32] and the investigation of the radiation/turbulence interaction [33].

The wide band model that will be examined in the present study is the Exponential Wide Band (EWB) due to Edwards and co-workers [34–36]. The modified parameters for the H_2O rotational band proposed by Modak [37] will be adopted. Other improvements that have been proposed for this model are due to Komornicki and Tomeczek [38], concerning the shape of the wide bands, due to Tien and coworkers [39–42], who provided wide band parameters for various species and due to Lallemant and Weber [43], who estimated coefficients of simple polynomial fits for the fast calculation of the line-width to spacing ratio parameter. The EWB model has been used in Ref. [5] to estimate WSGG parameters.

In inhomogeneous and nonisothermal media, band models are strictly applicable along a line of sight. Their extension to problems having more dimensions requires the explicit definition of the paths for which they will be applied. This is necessary in order to consistently construct the curves of growth along the propagation directions. The planar geometry is the simplest case that still requires the definition of directions which will be used in the angular integration of the radiative intensity. For this geometry, Zhang et al. [44] were the first to emphasise the effect of spectral correlations by applying the Malkmus model. Kim et al. [45], based on the observations of the previous authors, defined and solved a set of benchmark problems concerning the application of band models in planar media. These problems have been solved in Refs. [46–48] and [16,17], while new problems for reflecting walls have been added in Refs. [49,50]. Solutions for this set of benchmark problems will also be presented in this article. Noteworthy is the fact that only few studies deal with methods for applying band models consistently in multidimensional problems. Among them are the discrete direction method of Zhang et al. [44] and the Reverse Monte Carlo (RMC) of Walters and Buckius [51].

Motivated by these observations, the first objective of the present study is to formulate the application of the band models in such a way that their extension to multidimensional geometries will be straightforward. The proposed formulation decomposes a multidimensional problem in an equivalent set of one-dimensional problems, each one of them describing the propagation of a ray into the considered geometry. Investigation of the properties of the scaling procedure, which is necessary for the application of band models in inhomogeneous and nonisothermal media, shows that reduction of the computational requirements is achievable by efficiently combining the ray tracing and the scaling steps in the proposed formulation.

The second objective is to compare those of the band models that are most commonly used in engineering applications. For that purpose, the Goody and the Malkmus SNB and the Edwards EWB models are applied for the benchmark problems of Kim et al. [45].

A crucial point for the quality of the narrow band models is the set of the narrow band parameters used. In order to assess the sensitivity of the presented methods on this factor, two databases, namely the one published by Ludwig et al. [52] and the other in Refs. [19,30], are used and compared. A further assessment concerning the correlated versus. non-correlated applications of the band models is also discussed in the following sections.

2. Formulation

The planar geometry considered in the present work is depicted in Fig. 1(a). It consists of two infinite, parallel, non-reflecting boundaries which enclose an absorbing and emitting real gas layer of thickness L. The geometry is subdivided into N sublayers and the polar angle ϑ into N_m angular intervals $\Delta\vartheta_m$. Each of the intervals $\Delta\vartheta_m$ around ϑ_m is thought to surround a ray which starts from any point at the interface between two sublayers. The aim is to determine the net radiative flux q_x:

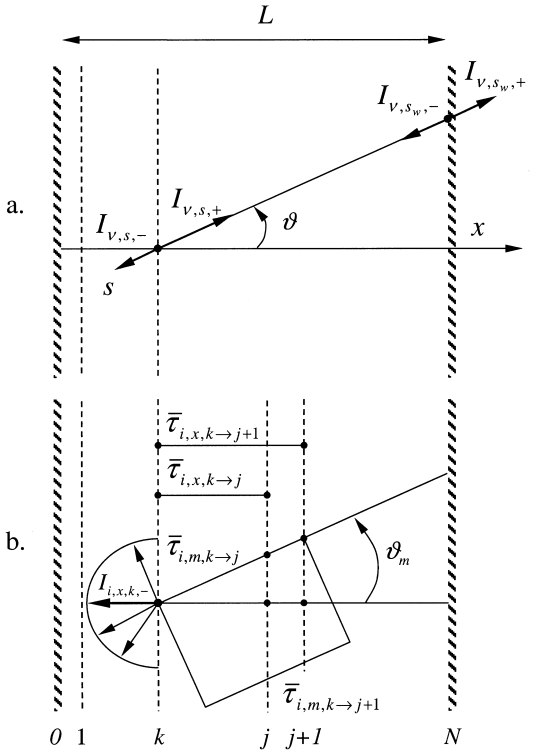

Fig. 1. Arrangement (a) and discretisation (b) of the planar geometry.

$$q_x = \int_0^\infty \int_{4\pi} I_{\nu,s}\cos\vartheta \,\mathrm{d}\Omega\,\mathrm{d}\nu = 2\pi\int_0^\infty\int_0^{\pi/2} I_{\nu,s,+}\cos\vartheta\sin\vartheta\,\mathrm{d}\vartheta\,\mathrm{d}\nu + 2\pi\int_0^\infty\int_{\pi/2}^{\pi} I_{\nu,s,-}\cos\vartheta\sin\vartheta\,\mathrm{d}\vartheta\,\mathrm{d}\nu \quad (1)$$

In Eq. (1), $I_{\nu,s}$ is the monochromatic radiative intensity in direction s and the subscripts $+$ and $-$ denote the positive and the negative traversing of the ray. For convenience, only the negative orientation will be examined. The direct numerical integration of Eq. (1) is:

$$q_{x,-} = 2\pi\int_0^\infty\int_{\pi/2}^{\pi} I_{\nu,s,-}\cos\vartheta\sin\vartheta\,\mathrm{d}\vartheta\,\mathrm{d}\nu \approx 2\pi\sum_{i=1}^{N_i}\sum_{m=1}^{N_m}\bar{I}_{i,m,k,-}\cos\vartheta_m\sin\vartheta_m\,\Delta\vartheta_m\,\Delta\nu_i \quad (2)$$

where $\bar{I}_{i,m,k,-}$ is the mean radiative intensity over the frequency interval $\Delta\nu_i$ at location k, angle ϑ_m and negative orientation. To solve Eq. (2), a method is needed to determine $\bar{I}_{i,m,k,-}$. For an absorbing, emitting and non-scattering medium, the radiative transfer equation along direction s is:

$$\frac{\partial I_{\nu,s}}{\partial s} = -\kappa_{\nu,s} I_{\nu,s} + \kappa_{\nu,s} I_{b,\nu,s} \quad (3)$$

where $\kappa_{\nu,s}$ is the monochromatic absorption coefficient and $I_{b,\nu,s}$ is the monochromatic blackbody radiative intensity. In Eq. (3), the in-scattering and out-scattering terms have been omitted. This is an acceptable approximation for the majority of combustion applications. A discussion about the influence of scattering in coal combustion applications is found in Refs. [53,54]. With reference to the arrangement of Fig. 1(a), the solution of Eq. (3) is known to be:

$$I_{\nu,s,-} = I_{\nu,s_w,-}\tau_{\nu,s_w\to s} + \int_{s_w}^{s} I_{b,\nu,s'}\left(\frac{\partial\tau_{\nu,s'\to s}}{\partial s'}\right)\mathrm{d}s' \quad (4)$$

where $I_{\nu,s_w,-}$ is the monochromatic intensity leaving the boundary and $\tau_{\nu,s'\to s}$ is the monochromatic transmissivity between a pair of points belonging to the examined ray. Eq. (4) is appropriate for LBL calculations. For the planar geometry, this method has been applied in Refs. [8,15,16,30]. The solution of Eq. (4) becomes more tractable if the typical in band modelling spectral averaging is applied (Ludwig et al. [52], Edwards [36]). Under the assumption of high emissivity walls, $I_{\nu,s_w,-}\to I_{b,\nu,s_w}$ and Eq. (4) is transformed into:

$$\bar{I}_{i,\,s,\,-} = \bar{I}_{\mathrm{b},\,i,\,s_w}\bar{\tau}_{i,\,s_w\to s} + \int_{s_w}^{s} \bar{I}_{\mathrm{b},\,i,\,s'}\left(\frac{\partial\bar{\tau}_{i,\,s'\to s}}{\partial s'}\right)\mathrm{d}s' \qquad (5)$$

where the overbars denote averaged quantities within the i-th spectral interval. As depicted in Fig. 1(b), a ray that starts from point k and is oriented towards the positive s direction has $N - k + 1$ intersection points until it reaches the wall. This ray can be decomposed into $N - k$ piecewise homogeneous and isothermal elements. Under this arrangement, the discrete form of Eq. (5) is:

$$\bar{I}_{i,\,m,\,k,\,-} = \bar{I}_{b,\,i,\,N}\,\bar{\tau}_{i,\,m,\,N\to k} + \sum_{j=N}^{k+1}\bar{I}_{b,\,i,\,j-1/2}\left(\bar{\tau}_{i,\,m,\,j-1\to k} - \bar{\tau}_{i,\,m,\,j\to k}\right) \qquad (6)$$

Eq. (6) is the basis for the proposed ray tracing formulation. The algorithmic implementation of this formulation consists of a forward and a backward step. The forward step defines the travelling lengths of the ray within each sublayer. In a inhomogeneous and nonisothermal medium, this step also includes the determination of equivalent band parameters according to a scaling procedure (Curtis–Godson approximation, or wide-band scaling) that will be presented below. Following the forward propagation of the ray, the transmissivities $\bar{\tau}_{i,\,m,\,k\to k+1},\cdots,\ \bar{\tau}_{i,\,m,\,k\to j},\cdots,\ \bar{\tau}_{i,\,m,\,k\to N}$ are calculated and stored. The forward step ends when the ray reaches the bounding wall. Then the interchange of variables $\bar{\tau}_{i,\,m,\,k\to j}=\bar{\tau}_{i,\,m,\,j\to k}$ is made, a procedure that is valid for the band models as will be shown later. After that step, all terms in Eq. (6) are known and the backward traversing from the wall to point k determines the intensity $\bar{I}_{i,\,m,\,k,\,-}$. This procedure is repeated for all frequency and angular intervals allowing the determination of the flux $q_{x,\,-}$ of Eq. (2). In a multidimensional geometry, this two step formulation is also applicable; the difference is that in the first step the rays are traced in the multidimensional instead of the planar space.

The ray tracing method will be applied in combination with the Goody [23,55] and the Malkmus [24] SNB models and the Edwards [36] EWB model. For the narrow band models, the curves of growth are:

$$\tau_{\mathrm{G}} = \exp\left(-ku\Big/\sqrt{1+\frac{ku}{4a}}\right) \qquad (7)$$

and

$$\tau_{\mathrm{M}} = \exp\left(-2a\left(\sqrt{1+\frac{ku}{a}}-1\right)\right) \qquad (8)$$

where u is the optical length, $k = S/d$ is the ratio of the line intensity S to the line spacing d and $a = \gamma/d$ is the line width γ to the spacing parameter. All the quantities in Eqs. (7) and (8) are averaged over a narrow spectral interval. The curve of growth of the EWB model is:

$$\tau_{\mathrm{E}} = \frac{u_{\mathrm{H}}}{A^*}\frac{\mathrm{d}A^*}{\mathrm{d}u_{\mathrm{H}}} \qquad (9)$$

where u_{H} is the optical length at a band head and A^* is the dimensionless band absorption given as a function of β, the line overlap parameter, by the four-region expression [35,36]:

$$A^* = \begin{cases} u_{\mathrm{H}}, & u_{\mathrm{H}}\le 1, \quad u_{\mathrm{H}}\le\beta \\ 2\sqrt{\beta u_{\mathrm{H}}}-\beta, & \beta\le u_{\mathrm{H}}\le 1/\beta, \quad \beta\le 1 \\ \ln(u_{\mathrm{H}}\beta)+2-\beta, & 1/\beta\le u_{\mathrm{H}}, \quad \beta\le 1 \\ \ln(u_{\mathrm{H}})+1, & u_{\mathrm{H}}\ge 1, \quad \beta\ge 1 \end{cases} \qquad (10)$$

For inhomogeneous and nonisothermal paths, the parameters appearing in the narrow band curves of growth are scaled according to the Curtis–Godson (CG) [56] approximation:

$$\tilde{u}_{s'\to s} = \int_{s'}^{s} p_{s''}\,\mathrm{d}s'' \approx \sum_{n=k}^{j} p_n\,s_n = \tilde{u}_{m,\,k\to j} \qquad (11)$$

$$\tilde{k}_{\nu,\,s'\to s} = \frac{1}{\tilde{u}_{s'\to s}}\int_{s'}^{s} k_{\nu,\,s''}\,p_{s''}\,\mathrm{d}s'' \approx \frac{\sum_{n=k}^{j} k_{i,\,n}\,p_n\,s_n}{\sum_{n=k}^{j} p_n\,s_n} = \tilde{k}_{i,\,m,\,k\to j} \qquad (12)$$

$$\tilde{a}_{\nu,\,s'\to s} = \frac{1}{\tilde{u}_{s'\to s}\,\tilde{k}_{\nu,\,s'\to s}}\int_{s'}^{s} a_{\nu,\,s''}\,k_{\nu,\,s''}\,p_{s''}\,\mathrm{d}s'' \approx \frac{\sum_{n=k}^{j} a_{i,\,n}\,k_{i,\,n}\,p_n\,s_n}{\sum_{n=k}^{j} k_{i,\,n}\,p_n\,s_n} = \tilde{a}_{i,\,m,\,k\to j} \qquad (13)$$

In Eqs. (11)–(13), n denotes the elements of a ray and the symbol $\sim$ the scaled quantities. An averaging procedure which is similar to Eqs. (11)–(13), termed wide band scaling [36], is applied to the parameters of the EWB model.

The CG approximation has three significant properties relevant to the ray tracing formulation. The first property is that:

$$\tilde{u}_{m,\,k\to j} = \tilde{u}_{m,\,j\to k}, \qquad \tilde{k}_{i,\,m,\,k\to j} = \tilde{k}_{i,\,m,\,j\to k}, \qquad \tilde{a}_{i,\,m,\,k\to j} = \tilde{a}_{i,\,m,\,j\to k} \qquad (14)$$

and therefore $\bar{\tau}_{i,m,k\to j} = \bar{\tau}_{i,m,j\to k}$ as it has been assumed for the derivation of Eq. (6). This property refers to a ray and it is valid for the application of the ray tracing formulation both in planar and in multidimensional geometries.

The second property allows the reuse of the computed correlations and it is explained below. Consider that the narrow band parameters have been computed for point k. Then, the CG-scaled optical length for point $k-1$ is:

$$\tilde{u}_{m,k-1\to j} = \sum_{n=k-1}^{j} p_n\, s_n = p_{k-1}\, s_{k-1} + \sum_{n=k}^{j} p_n\, s_n = p_{k-1}\, s_{k-1} + \tilde{u}_{m,k\to j} \tag{15}$$

Similarly, the CG-scaled mean line intensity to spacing parameter and the mean line width to spacing parameter for point $k-1$ are calculated based on the scaling of the previous point k:

$$\tilde{k}_{i,m,k-1\to j} = \frac{k_{i,k-1}\, p_{k-1}\, s_{k-1} + \tilde{k}_{i,m,k\to j}\, \tilde{u}_{m,k\to j}}{p_{k-1}\, s_{k-1} + \tilde{u}_{m,k\to j}} \tag{16}$$

$$\tilde{a}_{i,m,k-1\to j} = \frac{a_{i,k-1}\, k_{i,k-1}\, p_{k-1}\, s_{k-1} + \tilde{a}_{i,m,k\to j}\, \tilde{k}_{i,m,k\to j}\, \tilde{u}_{i,m,k\to j}}{k_{i,k-1}\, p_{k-1}\, s_{k-1} + \tilde{k}_{i,m,k\to j}\, \tilde{u}_{i,m,k\to j}} \tag{17}$$

This second property allows a unique traversing of a ray to generate all the necessary correlations between the ray elements. For both planar and multidimensional geometries, this property allows the efficient and yet rigorous evaluation of the radiative flux distribution. That happens because the amount of the necessary calculations per ray increases in the proposed formulation according to N and not according to N^2, as it happens in previous formulations. In addition, for a multidimensional problem, further reduction of the computational requirements can be achieved by the approximate reuse of the correlations produced for previously traced rays. However, this development will be detailed in a forthcoming publication.

The third property is strictly applicable for the planar geometry and it reduces the necessary estimations of k and a only along the normal ray.

$$\tilde{u}_{s'\to s} = \int_{s'}^{s} p_{s''}\, \mathrm{d}s'' = \frac{1}{\mu}\int_{x'}^{x} p_{x''}\, \mathrm{d}x'' = \frac{1}{\mu}\tilde{u}_{x'\to x} \tag{18}$$

$$\tilde{k}_{\nu,s'\to s} = \frac{1}{\tilde{u}_{s'\to s}}\int_{s'}^{s} k_{\nu,s''}\, p_{s''}\, \mathrm{d}s'' = \frac{\mu}{u_{x'\to x}}\frac{1}{\mu}\int_{x'}^{x} p_{x''}\, k_{\nu,x''}\, \mathrm{d}x'' = \tilde{k}_{\nu,x'\to x} \tag{19}$$

$$\tilde{a}_{\nu,s'\to s} = \frac{1}{\tilde{u}_{s'\to s}\tilde{k}_{\nu,s'\to s}}\int_{s'}^{s} a_{\nu,s''}\, k_{\nu,s''}\, p_{s''}\, \mathrm{d}s'' = \frac{\mu}{\tilde{u}_{x'\to x}\tilde{k}_{\nu,x'\to x}}\frac{1}{\mu}\int_{x'}^{x} a_{\nu,x''}\, k_{\nu,x''}\, p_{x''}\, \mathrm{d}x'' = \tilde{a}_{\nu,x'\to x} \tag{20}$$

This property drastically simplifies the numerical integration over the polar angle in Eq. (2) because it allows the subsequent evaluation of the curves of growth for the N_m rays based on band parameters which have been scaled once for the normal ray and optical length which is readily scaled through Eq. (18).

3. Results

The ray tracing formulation is applied for the set of problems summarised in Table 1. These cases were first presented by Kim et al. [45] as basic configurations for the evaluation of the radiative source term in a planar geometry containing a H_2O/N_2 mixture at 1 atm total pressure. In cases 1 and 2, the medium is homogeneous ($P_{tot} = P_{H_2O} = 1$ atm) and isothermal and the distance between the infinite parallel plates is 0.1 and 1.0 m, respectively. Comparisons between the results for case 1 and 2 show the influence of the optical length on the distribution of the radiative source terms. Cases 3 and 5 are again homogeneous, but the temperature profiles are of a boundary layer and of a parabolic type, respectively. In case 4, the temperature is uniform, the H_2O concentration follows a parabolic profile and N_2 is mixed up to the total pressure of 1 atm.

The problems have been solved by Kim et al. [45]

Table 1
Specification of the examined cases[a]

Case	Description	L (m)	T_{H_2O} (K)	P_{H_2O} (atm)
1	Homogeneous, isothermal	0.1	1000	1
2	Homogeneous, isothermal	1.0	1000	1
3[b]	Boundary layer	0.2	Ref. [45]	1
4	Parabolic concentration	1.0	1000	Ref. [45]
5[c]	Parabolic temperature	0.4	Ref. [45]	1

[a] For all cases, $P_{tot} = 1$ atm, $\varepsilon_w = 1.0$.
[b] For case 3, $T_0 = 1500$ K and $T_N = 300$ K.
[c] For case 5, $T_0 = T_N = 400$ K.

using an S-20 method which was reformulated to include transmissivity as the radiative property characterising the non-gray gas. Therefore their method was capable to incorporate band models. They presented results using the Malkmus SNB and the Edwards EWB models. The same problems have been solved in Refs. [46–48] using the Malkmus SNB and in Refs. [16,17] using the SLW model combined with a discrete ordinates formulation. In this section, results will be presented using the ray tracing formulation in combination with the Goody and the Malkmus SNB models and the Edwards EWB model. Two databases describing the spectral variation of k, the mean line intensity to spacing parameter, and $1/d$, the inverse of the line spacing, have been used. The first one, denoted LMRT (Ludwig, Malkmus, Reardon, Thompson), has been published in [52] and the second one, denoted HL^{2}ST (Hartmann, Levi Di Leon, Soufiani, Taine), is available in Refs. [19,30]. The third narrow band parameter, the line halfwidth γ, is given either as:

$$\gamma_{\mathrm{H_2O,\ LMRT}} = 0.44 P_{\mathrm{H_2O}} \frac{273}{T} + 0.09 P_{\mathrm{tot}} \sqrt{\frac{273}{T}} \tag{21}$$

or

$$\gamma_{\mathrm{H_2O,\ HL^2ST}} = 0.462 P_{\mathrm{H_2O}} \frac{296}{T} + 0.0792 P_{\mathrm{tot}} \sqrt{\frac{296}{T}} \tag{22}$$

In order to show the differences between these two databases, results for the five problems are presented using the Goody SNB model in combination with both of them. The influence of adopting different narrow band models is shown by comparing the results obtained with the Goody and the Malkmus SNB models and the narrow band parameters from the HL^{2}ST database. In addition, results will be presented using the narrow band models following either the exact Eq. (6) or the non-correlated equation:

$$\bar{I}_{i,\,m,\,k-1,\,-} = \bar{I}_{i,\,m,\,k,\,-}\,\bar{\tau}_{i,\,m,\,k-1\to k} + \bar{I}_{b,\,i,\,k-1/2}\left(1-\bar{\tau}_{i,\,m,\,k-1\to k}\right) \tag{23}$$

Noteworthy is the fact that by omitting the spectral dependency, Eq. (23) becomes the basis of the discrete transfer method as it was originally described by Lockwood and Shah [57]. The same equation has been applied together with the EWB model by Doherty and Fairweather [58] and Cumber et al. [59] and with the Malkmus SNB model by Miranda and Sacadura [47] and Liu et al. [48].

Only the exact Eq. (6) is used together with the EWB model. Following Edwards [36], the width of each band is estimated as $\Delta\nu = A/(1-\bar{\tau}_{\mathrm{E}})$, where A is the integrated band absorption, and the mean band transmissivity $\bar{\tau}_{\mathrm{E}}$ is given from Eqs. (9) and (10). In the ray tracing formulation, the wide band parameters are scaled in a very similar way as in Eqs. (11)–(13) when ray elements are added in a solution of Eq. (6). However, even in a homogeneous and isothermal problem, there is a mismatch of the band spectral widths for the correlated transmissivities of two consecutive ray el-

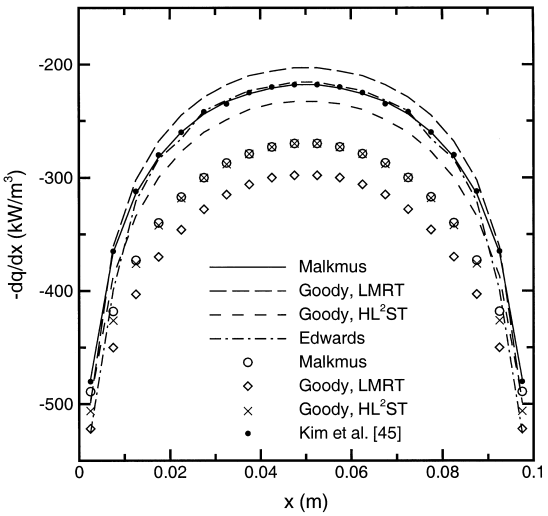

Fig. 2. Radiative source terms for the homogeneous and isothermal problem with optical length 0.1 m (case 1, Table 1). Lines correspond to correlated solutions, open symbols to non-correlated solutions and dots to the correlated S-20 solution of Ref. [45] using the Malkmus SNB model.

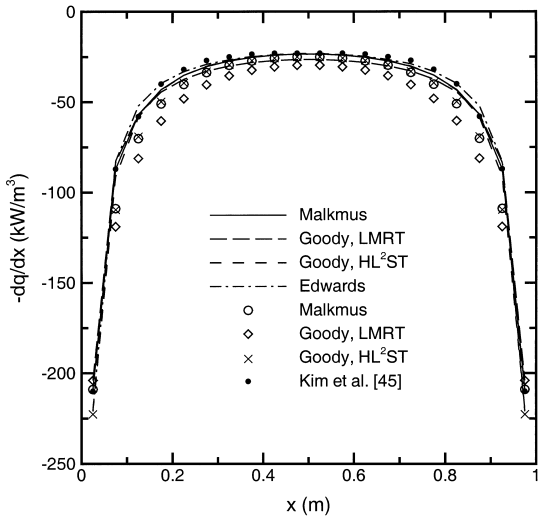

Fig. 3. Radiative source terms for the homogeneous and isothermal problem with optical length 1 m (case 2, Table 1). Lines correspond to correlated solutions, open symbols to non-correlated solutions and dots to the correlated S-20 solution of Ref. [45] using the Malkmus SNB model.

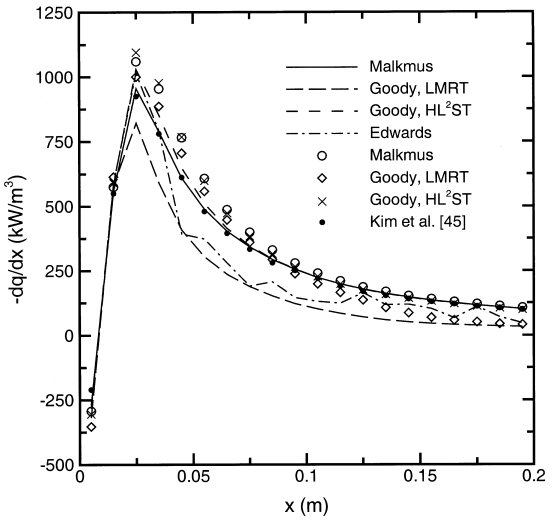

Fig. 4. Radiative source terms for the boundary-layer type temperature distribution of pure H_2O (case 3, Table 1). Lines correspond to correlated solutions, open symbols to non-correlated solutions and dots to the correlated S-20 solution of Ref. [45] using the Malkmus SNB model.

ements. This problem will be further analysed in a subsequent paragraph. In order to take the optical length to band-width dependency into account, an algorithm has been implemented that treats the bands of two consecutive ray elements as independent, calculating the transmissivities in the resulting overlapping and nonoverlapping regions as suggested in Ref. [36]. This algorithm is a rigorous implementation of Eq. (6) within the frame of a wide band model, but it also diminishes any advantage of the EWB over the SNB models with respect to computational efficiency.

The same spatial and angular discretisation has been adopted for all the examined test cases. The planar geometry was subdivided into 20 sublayers and the polar angle into 24 angular intervals. The distributions of the radiative source terms for the cases 1 to 5 are given in Figs. 2–6, respectively. In every figure, eight lines are plotted. The first four lines correspond to the application of Eq. (6) with: (a) the Malkmus model and narrow band parameters from the HL^2ST database, (b) the Goody model with LMRT parameters, (c) the Goody model with HL^2ST parameters and (d) the EWB model with parameters from Ref. [36] except of the rotational band, which is modelled according to [37]. The next three lines are solutions obtained from the non-correlated Eq. (23) and the Malkmus and Goody models with parameters as in the three first cases mentioned previously. The eighth line in Figs. 2–5 corresponds to the correlated S-20 solution of Kim et al. in combination with the Malkmus model and the HL^2ST database. Their solution has been omitted in Fig. 6 because the authors have solved case 5 using only a subset of the narrow band database. That was done in order to compare their method with previously published results in Ref. [44]. The general shapes of the lines for all the cases have been explained by Kim et al. [45]. The subsequent discussion is focused on the

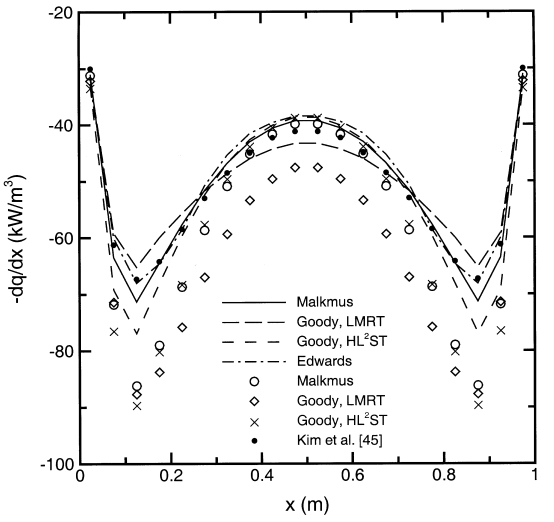

Fig. 5. Radiative source terms for the isothermal problem with parabolic H_2O concentration (case 4, Table 1). Lines correspond to correlated solutions, open symbols to non-correlated solutions and dots to the correlated S-20 solution of Ref. [45] using the Malkmus SNB model.

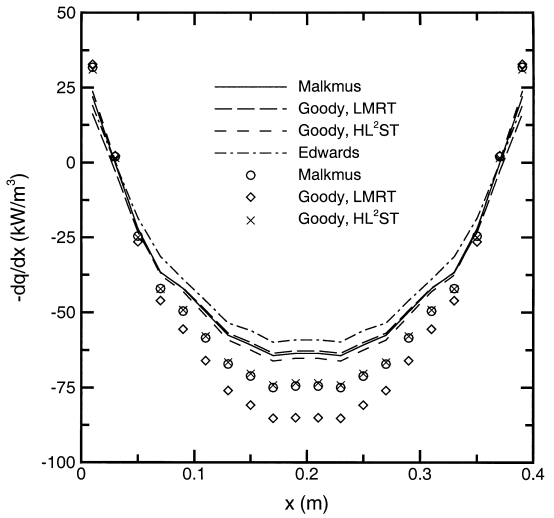

Fig. 6. Radiative source terms for the parabolic temperature distribution of pure H_2O (case 5, Table 1). Lines correspond to correlated solutions and symbols to non-correlated.

distinctions between correlated versus non-correlated results, narrow versus wide band modelling, Goody versus Malkmus SNB models and LMRT versus HL^{2}ST databases.

The first observation is that the correlated solutions differ significantly from the non-correlated ones. This is clearly evident in Figs. 2, 5 and 6. In case 2, the significant optical length together with the uniform composition and temperature distributions bring the central sublayers into radiative equilibrium, where the radiative sources calculated by all the examined variants should be indistinguishable as tending to zero. However, even in case 2, the radiative source terms of the correlated and non-correlated solutions for the outer sublayers are in disagreement. For case 3 and Fig. 4, this disagreement is identified for the results of the Goody model with LMRT parameters.

A second observation is that the non-correlated solutions obtained with the Goody and the Malkmus models and a common database for the narrow band parameters are almost identical. This is evident in all the examined cases. The explanation is that:

$$\lim_{u\to 0}\tau_{\mathrm{G}} = \lim_{u\to 0}\tau_{\mathrm{M}} = \exp(-ku) \tag{24}$$

where $\exp(-ku)$ is the transmissivity at the weak line limit. Taking into account the fact that when the spatial discretisation is improved, the optical length tends to approach zero; therefore the non-correlated transmissivity $\bar{\tau}_{i,\,m,\,k-1\to k}$ in Eq. (23) can be approximated by $\exp(-k_{i,\,k-1\to k}u_{m,\,k-1\to k})$. This expression solely depends on the thickness of a sublayer. In contrast, the correlated solutions correctly allow the transmissivity to assume values not only in the weak line regime, but also in the strong line limit, as well as in the transition region between both. This is achieved because the optical length increases when subsequent ray elements are added to the CG-scaling and consequently, the Goody and the Malkmus curves of growth depart from the weak line limit. In this intermediate region between the weak and the strong line limits the two SNB models do not exhibit an identical behaviour. This is the reason why, in contrast to the non-correlated solutions, there are differences in the results obtained from the correlated approach together with the Goody and the Malkmus models and the common HL^{2}ST database.

A third observation is that there are significant differences between the two narrow band databases. These differences are evident for both the correlated and the non-correlated solutions. However, it should be noted that the non-correlated cases highlight the differences between the two databases. This is because the results in these cases, as mentioned earlier, correspond to the weak line limit. It is exactly this limit, together with the strong line one, that are used in deducing the narrow band parameters from experimental or theoretical spectra of higher resolution.

The fourth observation concerns the implementation of the EWB model. The model has been used only within the correlated formulation. For all the cases, it gave results in good agreement with the correlated applications of the SNB models. This is especially true for cases 1, 2 and 4, where there was no incoming radiation at the boundaries. For case 5 and especially for case 3, where the boundaries emit significantly, the EWB predicted non-smooth distribution of the radiative source term. In general, this problem is attributed to the inability of the EWB model to treat accurately the radiant transfer in the spectral regions of the band wings. In order to explain that, case 3 is considered. In this case, a part of the strong wall emission is transmitted through the wall neighbouring sublayers without being attenuated. This transmission takes place because of the spectral windows between the box-shaped bands. As ray elements are added to the wide band scaling, the correlated band width also increases. It is therefore possible for the correlated band transmissivity of a distant from the wall element to become wider than the band transmissivity corresponding to the previous path elements. That will result the illumination of the box-band sides by the wall radiation transmitted through the spectral windows. Taking into account the fact that according to Eq. (6), the radiative intensity depends on the difference of the transmissivities between adjacent elements, this behaviour of the wide band model may lead to unsatisfactory prediction of the local source term. In contrast, SNB models evaluate the local $\Delta\bar{\tau}$ of Eq. (6) in fixed spectral intervals. Therefore, the previous physically unrealistic mechanism is avoided because wall radiation is transmitted to an inner path element after being attenuated by the band wings of the intervening sublayers.

Table 2 summarises the net wall fluxes for the five examined cases and the seven implementations of the ray tracing method. The discrepancy between the correlated and the non-correlated solutions is evident for all the combinations. The LMRT database, when applied to the Goody model in a correlated solution, predicts lower wall fluxes compared to the results of the corresponding applications of the HL^{2}ST database. This tendency is reversed in the non-correlated solutions, with the exception of case 3. The wall fluxes predicted by the EWB model are generally lower compared with the correlated applications of SNB models. The same observation, with the exception of case 3, applies comparing the Malkmus against the Goody model. However, it should be noted that the level of agreement between the predictions of the wall fluxes obtained from the correlated applications of the band models is satisfactory. Finally, the wall fluxes calculated by the ray tracing method, the Malkmus SNB

model and the HL^{2}ST database for cases 1 to 4 are in good agreement with the results of Kim et al. [45]. The slight discrepancies are attributed to the different angular discretisation; in Ref. [45] 20 discrete ordinates are accepted, while in the present study the polar angle has been subdivided into 24 intervals.

4. Discussion and conclusions

In this article, various alternatives for incorporating band models in a ray tracing formulation have been examined. These alternatives include narrow versus wide band models, correlated versus non-correlated solutions, as well as two narrow band models and two databases for their parameters.

It was found that results using the EWB model were in generally good agreement with the SNB models. However, taking the spectral correlations for the EWB model fully into account requires tracking of the band width variation along a path. This implies the use of an algorithm for defining the overlapping regions of the bands of two consecutive ray elements. That essentially cancels the advantage in computer time of the EWB over the SNB models. In addition, although calculations in a EWB implementation concern only few wide spectral intervals (11 in a CO_2/H_2O mixture), the estimation of the band parameters is a procedure much more demanding in computer time compared to narrow band models. An approximate implementation of the EWB model is feasible, based on fixed band widths and (along the line of Ref. [43]) on simplified curve fits of the wide band parameters. However, such an implementation should be compared with a narrow band model solution with reduced spectral resolution; e.g., 45 spectral intervals, as in Ref. [8], instead of 217 (HL^{2}ST) or 299 (LMRT) intervals used in the present study. Nevertheless, the EWB model is a useful model in many engineering applications, especially for species which have known wide band parameters and unknown narrow band datasets.

Significant discrepancies were observed between the correlated and the non-correlated solutions. The latter have been used by some authors as an alternative to reduce the computational requirements of band models. The problem originates from the fact that the scaling of the band parameters may lead to excessive computer times. Non-correlated solutions answer this problem by omitting the scaling procedure. That is physically unrealistic. In addition, it is not essential any more because the recursive calculation of the scaled band parameters proposed in this study reduces significantly the computational requirements of a correlated band implementation. Therefore, the adoption of the non-correlated approach is not recommended.

The Goody and the Malkmus SNB models have been compared by Soufiani et al. [30]. It was found in this reference that the Malkmus model gave results in closer agreement to LBL calculations. In the present study there are no data of higher accuracy than the band models (LBL results, or measured spectra) to serve as criterion for comparisons. Therefore, the superiority of the Malkmus over the Goody model can not be questioned. It should be mentioned that there is a theoretical reasoning supporting the finding of Ref. [30]; the Malkmus curve of growth has a wider transition region between the strong and the weak line limits. In high temperature applications, this attribute is believed to represent better the influence of the hot lines on the transmissivity of the medium. However, it should also be noted that, among the examined band model implementations, the least discrepancies were observed for the cases where the two SNB models were applied with a common narrow band database. Taking into account the significantly simpler mathematics associated with the Goody model, the last observation leads to the conclusion that this SNB model is still useful. That is especially true in cases such as the inclusion of scattering in band models where further mathematical development is required [60].

The discrepancies between the results obtained from the LMRT and the HL^{2}ST databases were found to be

Table 2
Net wall flux (kW/m^2)

Model	Case 1	Case 2	Case 3	Case 4	Case 5
Malkmus, correlated	−14.2	−28.1	278.1	−25.5	−7.5
Goody, LMRT, correlated	−13.7	−28.5	276.0	−25.3	−7.6
Goody, HL^{2}ST, correlated	−15.1	−29.0	277.6	−26.4	−7.7
Edwards, correlated	−14.6	−27.6	272.6	−24.8	−6.9
Malkmus, non-correlated	−16.7	−31.1	277.6	−28.7	−8.6
Goody, LMRT, non-correlated	−18.2	−34.1	275.4	−31.4	−9.7
Goody, HL^{2}ST, non-correlated	−16.8	−31.2	277.3	−28.8	−8.5
Kim et al. [45], Malkmus correlated	−14.3	−28.2	277.4	−25.4	–[a]

[a] Not cited because for this case, in Ref. [45], only a subset of the HL^{2}ST database was used.

significant. Future work should use and evaluate the newer database available in Ref. [11]. However, it should be mentioned that this database contains parameters fitted to the Malkmus model, while the parameters in the two examined databases have been determined from first principles, independently of any SNB model. Therefore, the conditions under which this new database is applicable for the Goody model should carefully be examined. Nevertheless, future work should focus on the efficient implementation of the presented ray tracing method to multidimensional problems.

Acknowledgements

Part of this work was financially supported by the Commission of the European Communities under the JOULE II CT92-153 project "Evaluation of Pressurised Pulverised Coal Combustion with CO_2 recirculation". The author would also like to acknowledge the Institute of Fluid Mechanics of the University of Erlangen–Nürnberg for hosting him within the EU-funded TMR CT-98-224 RADIARE network.

References

[1] H.C. Hottel, A.F. Sarofim, Radiative Transfer, McGraw-Hill, New York, 1967.
[2] M.F. Modest, The weighted-sum-of-gray-gases model for arbitrary solution methods in radiative transfer, J. Heat Transfer 113 (1991) 650–656.
[3] T.H. Song, Comparison of engineering models of non-gray behavior of combustion products, Int. J. Heat Mass Transfer 36 (1993) 3975–3982.
[4] P.B. Taylor, P.J. Foster, The total emissivities of luminous and non-luminous flames, Int. J. Heat Mass Transfer 17 (1974) 1591–1605.
[5] T.F. Smith, Z.F. Shen, J.N. Friedman, Evaluation of coefficients for the weighted sum of gray gases model, J. Heat Transfer 104 (1982) 602–608.
[6] A. Soufiani, E. Djavdan, A comparison between weighted sum of gray gases and statistical narrow-band radiation models for combustion applications, Combust. Flame 97 (1994) 240–250.
[7] N. Lallemant, A. Sayre, R. Weber, Evaluation of emissivity correlations for H_2O–CO_2–N_2/air mixtures and coupling with solution methods of the radiative transfer equation, Prog. Energy Combust. Sci. 22 (1996) 543–574.
[8] L. Pierrot, A. Soufiani, J. Taine, Accuracy of the various gas IR radiative property models applied to radiative transfer in planar media, in: M.P. Mengüç (Ed.), Proceedings of the First International Symposium on Radiative Transfer, Begell House Inc., Kusadaci, Turkey, 1995, pp. 209–227.
[9] R. Goody, R. West, L. Chen, D. Crisp, The correlated-k method for radiation calculations in nonhomogeneous atmospheres, J. Quant. Spectrosc. Radiat. Transfer 42 (1989) 539–550.
[10] A. Lacis, V. Oinas, A description of the correlated-k distribution method for modeling non-gray gaseous absorption, thermal emission and multiple scattering in vertically inhomogeneous atmospheres, J. Geophys. Res. 96 (1991) 9027–9063.
[11] A. Soufiani, J. Taine, High temperature gas radiative property parameters of statistical narrow-band model for H_2O, CO_2 and CO and correlated-k model for H_2O and CO_2, Int. J. Heat Mass Transfer 40 (1997) 987–991.
[12] O. Marin, R.O. Buckius, Wide band correlated-k approach to thermal radiative transport in nonhomogeneous media, J. Heat Transfer 119 (1997) 719–729.
[13] O. Marin, R.O. Buckius, A simplified wide band model of the cumulative distribution function of water vapor, Int. J. Heat Mass Transfer 41 (1998) 2877–2892.
[14] O. Marin, R.O. Buckius, A simplified wide band model of the cumulative distribution function of carbon dioxide, Int. J. Heat Mass Transfer 41 (1998) 3881–3897.
[15] M.K. Denison, B.W. Webb, A spectral line-based weighted-sum-of-gray-gases model for arbitrary RTE solvers, J. Heat Transfer 115 (1993) 1004–1012.
[16] M.K. Denison, B.W. Webb, The spectral line-based weighted-sum-of-gray-gases model in nonisothermal nonhomogeneous media, J. Heat Transfer 117 (1995) 359–365.
[17] M.K. Denison, B.W. Webb, The spectral line weighted-sum-of-gray-gases model. A review, in: M.P. Mengüç (Ed.), Proceedings of the First International Symposium on Radiative Transfer, Begell House Inc., Kusadaci, Turkey, 1995, pp.193–208.
[18] J. Taine, A line-by-line calculation of low-resolution radiative properties of CO_2–CO-transparent nonisothermal gases mixtures up to 3000 K, J. Quant. Spectrosc. Radiat. Transfer 30 (1983) 371–379.
[19] J.M. Hartmann, R. Levi Di Leon, J. Taine, Line-by-line and narrow-band statistical model calculations for H_2O, J. Quant. Spectrosc. Radiat. Transfer 32 (1984) 119–127.
[20] Ph. Riviere, S. Langlois, A. Soufiani, J. Taine, An approximate database of H_2O infrared lines for high temperature applications at low resolution. Statistical narrow-band parameters, J. Quant. Spectrosc. Radiat. Transfer 53 (1995) 221–234.
[21] L.S. Rothman, C.P. Rinsland, A. Goldman, S.T. Massie, D.P. Edwards, J-M. Flaud, A. Perrin, C. Camy-Peyret, V. Dana, J.-Y. Mandin, J. Schroeder, A. McCann, R.R. Gamache, R.B. Wattson, K. Yoshino, K.V.K. Chance, W. Jucks, L.R. Brown, V. Nemtchinov, P. Varanasi, The HITRAN molecular spectroscopic database and HAWKS (HITRAN Atmospheric Workstation): 1996 Edition, J. Quant. Spectrosc. Radiat. Transfer 60 (1998) 665–710.
[22] L.S. Rothman, HITRAN Newsletter 5 (1996) 1–4.
[23] R.M. Goody, A statistical model for water-vapor absorption, Quart. J. Royal Meteorol. Soc. 78 (1952) 165–169.
[24] W. Malkmus, Random Lorentz band model with expo-

nential-tailed S^{-1} line-intensity distribution function, J. Opt. Soc. Am. 57 (1967) 323–329.
[25] W.L. Grosshandler, Radiative heat transfer in nonhomogeneous gases: a simplified approach, Int. J. Heat Mass Transfer 23 (1980) 1447–1459.
[26] W.L. Grosshandler, H.D. Nguyen, Application of the total transmittance nonhomogeneous radiation model to methane combustion, J. Heat Transfer 107 (1985) 445–450.
[27] M.E. Kounalakis, Y.R. Sivathanu, G.M. Faeth, Infrared radiation statistics of nonluminus turbulent diffusion flames, J. Heat Transfer 113 (1991) 437–445.
[28] S.P. Fuss, O.A. Ezekoye, M.J. Hall, The absorptance of infrared radiation by methane at elevated temperatures, J. Heat Transfer 118 (1996) 918–923.
[29] B. Leckner, Spectral and total emissivity of water vapor and carbon dioxide, Combust. Flame 19 (1972) 33–48.
[30] A. Soufiani, J.M. Hartmann, J. Taine, Validity of band-model calculations for CO_2 and H_2O applied to radiative properties and conductive–radiative transfer, J. Quant. Spectrosc. Radiat. Transfer 33 (1985) 243–257.
[31] A. Soufiani, J. Taine, Application of statistical narrow band model to coupled radiation and convection at high temperature, Int. J. Heat Mass Transfer 30 (1987) 437–447.
[32] A. Soufiani, J. Taine, Experimental and theoretical studies of combined radiative and convective transfer in CO_2 and H_2O laminar flows, Int. J. Heat Mass Transfer 32 (1989) 477–486.
[33] F. Kritzstein, A. Soufiani, Infrared gas radiation from a homogeneously turbulent medium, Int. J. Heat Mass Transfer 36 (1993) 1749–1762.
[34] D.K. Edwards, W.A. Menard, Comparison of models for correlation of total band absorption, Appl. Optics 3 (1964) 621–626.
[35] D.K. Edwards, A. Balakrishnan, Thermal radiation by combustion gases, Int. J. Heat Mass Transfer 16 (1973) 25–40.
[36] D.K. Edwards, Molecular gas band radiation, in: T.F. Irvine Jr., J.P. Hartnett (Eds.), Advances in Heat Transfer, vol. 12, Academic Press, New York, 1976, pp. 115–193.
[37] A.T. Modak, Exponential wide band parameters for the pure rotational band of water vapor, J. Quant. Spectrosc. Radiat. Transfer 21 (1979) 131–142.
[38] W. Komornicki, J. Tomeczek, Modification of the wide-band gas radiation model for flame calculation, Int. J. Heat Mass Transfer 35 (1992) 1667–1672.
[39] C.L. Tien, M.F. Modest, C.R. McGreight, Infrared radiation properties of nitrous oxide, J. Quant. Spectrosc. Radiat. Transfer 12 (1972) 267–277.
[40] C.L. Tien, Band and total emissivities of ammonia, Int. J. Heat Mass Transfer 16 (1973) 856–857.
[41] M.A. Brosmer, C.L. Tien, Infrared radiation properties of methane at elevated temperature, J. Quant. Spectrosc Radiat. Transfer 33 (1985) 521–532.
[42] M.A. Brosmer, C.L. Tien, Thermal radiation properties of acetylene, J. Heat Transfer 107 (1985) 943–948.
[43] N. Lallemant, R. Weber, A computationally efficient procedure for calculating gas radiative properties using the exponential wide band model, Int. J. Heat Mass Transfer 39 (1996) 3273–3286.
[44] L. Zhang, A. Soufiani, J. Taine, Spectral correlated and non-correlated radiative transfer in a finite axisymmetric system containing an absorbing and emitting real gas–particle mixture, Int. J. Heat Mass Transfer 31 (1988) 2261–2272.
[45] T.K. Kim, J.A. Menart, H.S. Lee, Nongray radiative gas analyses using the *S–N* discrete ordinates method, J. Heat Transfer 113 (1991) 946–952.
[46] J. Liu, S.N. Tiwari, Investigation of radiative transfer in nongray gases using a narrow band model and Monte Carlo simulation, J. Heat Transfer 116 (1994) 160–166.
[47] Miranda A.B. De, J.F. Sacadura, An alternative formulation of the *S–N* discrete ordinates for predicting radiative transfer in nongray gases, J. Heat Transfer 118 (1996) 650–653.
[48] F. Liu, Ö.L. Gülder, G.J. Smallwood, Y. Ju, Non-grey gas radiative transfer analyses using the statistical narrow-band model, Int. J. Heat Mass Transfer 41 (1998) 2227–2236.
[49] J.A. Menart, H.S. Lee, T.K. Kim, Discrete ordinates solutions of nongray radiative transfer with diffusely reflecting walls, J. Heat Transfer 115 (1993) 184–193.
[50] J.A. Menart, H.S. Lee, Nongray gas analyses for reflecting walls utilizing a flux technique, J. Heat Transfer 115 (1993) 645–652.
[51] D.V. Walters, R.O. Buckius, Rigorous development for radiation heat transfer in nonhomogeneous absorbing, emitting and scattering media, Int. J. Heat Mass Transfer 35 (1992) 3323–3333.
[52] C.B. Ludwig, W. Malkmus, J.E. Reardon, J.A.L. Thompson, Handbook of Infrared Radiation, NASA SP-3080, Washington, DC, 1973.
[53] J.G. Marakis, C. Papapavlou, E. Kakaras, A parametric study of radiative heat transfer in pulverised coal furnaces, Int. J. Heat Mass Transfer 43 (2000) 2961–2971.
[54] J.G. Marakis, C. Papapavlou, G. Brenner, F. Durst, Monte Carlo simulation of a nephelometric experiment, Int. J. Heat Mass Transfer, accepted.
[55] R.M. Goody, Y.L. Yung, Atmospheric Radiation, 2nd ed., Oxford University Press, UK, Oxford, 1989.
[56] W.L. Godson, The evaluation of infra-red radiation fluxes due to atmospheric water vapour, Quart. J. Royal Meteorol. Soc. 79 (1953) 367–379.
[57] F.C. Lockwood, N.G. Shah, A new radiation solution method for incorporation in general combustion prediction procedures, Eighteenth Symp. (Int.) on Combustion, The Combustion Institute, 1981, pp. 1405–1414.
[58] P. Docherty, M. Fairweather, Predictions of radiative transfer from nonhomogeneous combustion products using the discrete transfer method, Combust. Flame 71 (1988) 79–87.
[59] P.S. Cumber, M. Fairweather, H.S. Ledin, Application of wide band radiation models to nonhomogeneous combustion systems, Int. J. Heat Mass Transfer 41 (1998) 1573–1584.
[60] W. Malkmus, Some comments on the extension of band models to include scattering, J. Quant. Spectrosc. Radiat. Transfer 40 (1988) 201–204.